

MRG-R1: Reinforcement Learning for Clinically Aligned Medical Report Generation

Pengyu Wang, Shuchang Ye, Usman Naseem, Jinman Kim Member, IEEE

Abstract—Medical report generation (MRG) aims to automatically derive radiology-style reports from medical images to aid in clinical decision-making. However, existing methods often generate text that mimics the linguistic style of radiologists but fails to guarantee clinical correctness, because they are trained on token-level objectives which focus on word-choice and sentence structure rather than actual medical accuracy. We propose a semantic-driven reinforcement learning (SRL) method for medical report generation, adopted on a large vision-language model (LVLM). SRL adopts Group Relative Policy Optimization (GRPO) to encourage clinical-correctness-guided learning beyond imitation of language style. Specifically, we optimise a report-level reward: a margin-based cosine similarity (MCCS) computed between key radiological findings extracted from generated and reference reports, thereby directly aligning clinical-label agreement and improving semantic correctness. A lightweight reasoning format constraint further guides the model to generate structured “thinking → report” outputs. We evaluate Medical Report Generation with Semantic-driven Reinforcement Learning (MRG-R1), on two datasets: IU X-Ray and MIMIC-CXR using clinical efficacy (CE) metrics. MRG-R1 achieves state-of-the-art performance with CE-F1 51.88 on IU X-Ray and 40.39 on MIMIC-CXR. We found that the label-semantic reinforcement is better than conventional token-level supervision. These results indicate that optimizing a clinically grounded, report-level reward—rather than token overlap—meaningfully improves clinical correctness. This work is a prior to explore semantic-reinforcement in supervising medical correctness in medical Large vision-language model (Medi-LVLM) training.

Index Terms—Medical Report Generation, Reinforcement Learning

I. INTRODUCTION

Automatic medical report generation (MRG) produces radiology-style narratives from medical images, documenting clinically relevant findings, impressions, and recommendations in a format familiar to clinicians. This is a timely and important technology, as clinicians face mounting challenges with the growing volume of imaging studies due to the increasing clinical use of medical imaging [1]. Efficiently interpreting large image sets and translating observations into comprehensive diagnostic reports requires significant expertise and time, motivating

efforts to automate this process. Even for experienced radiologists, the process is labor-intensive and vulnerable to error under workload pressure [2], missing subtle abnormalities or uncertainties mis-specified [3], and terminology applied inconsistently across cases. Moreover, modern imaging pipelines often introduce richer but more heterogeneous inputs, which compounds the cognitive load without proportionally increasing available reporting time. Against this backdrop, MRG has emerged as a promising approach to mitigate workload, improve efficiency, and enhance consistency and clinical fidelity.

Recently, automatic medical report generation has garnered significant interest and achieved substantial advances with deep learning applied to healthcare [4]–[8]. However, as reported in prior work [9], existing methods can generate fluent, radiologist-style report, but fail to ensure semantic consistency, which is important in clinical use. One of the key reason is that most existing models instead learn with token-level objectives: they decompose reporting into autoregressively predicting the next token, rewarding surface n-gram overlap. This makes it easy to generate sentences that look like radiology text but differ in meaning, for example, treating “no pneumothorax” and “small pneumothorax” as similarly plausible continuations if both match local style without enforcing consistency of clinical facts across the full report. Early MRG methods adopt encoder-decoder architectures with CNN backbones for visual features and LSTM/GRU decoders for sentence generation [7], [8], [10]. Transformers improve global context modeling and parallelization, helping capture dependencies across multiple sentences and sections and enabling stronger cross-modal alignment [6], [11]. More recently, large vision-language models (LVLMs), which couple high-capacity visual encoders with instruction-tuned language models, further enhance fluency and generalization in medical image-text tasks [4], [12], [13]. But across CNN-RNN, Transformer-based, and LVLM-based systems, the predominant training paradigm remains token-level likelihood. This focus on local word prediction encourages stylistic mimicry, hallucinated but plausible statements, and incomplete coverage, leaving report-level clinical correctness underconstrained and motivating objectives that act directly at the semantic, report level.

Building on this mismatch between token-level training and the clinical goals of report generation, producing factually correct, complete, and clinically meaningful in-

Corresponding author: Jinman Kim and Usman Naseem

Pengyu Wang, Shuchang Ye, and Jinman Kim are with the School of Computer Science, The University of Sydney, Camperdown, NSW 2006, Australia (email: pwang0442@uni.sydney.edu.au; shuchang.ye@sydney.edu.au; jinman.kim@sydney.edu.au).

Usman Naseem is with School of Computing, Macquarie University, Macquarie Park, NSW 2113, Australia (email: usman.naseem@mq.edu.au).

terpretations, recent work adds semantic supervision to better align text with image-based evidence (findings visually supported by the image). Contrastive learning aligns image-report pairs in a shared representation space; yet offers only global signals that overlook fine-grained phenomena and entity-relation structure [14]–[16]. Multi-task learning jointly trains classification/localization with report generation, providing explicit semantic anchors that improve coverage and inhibit hallucinations. However, labels are incomplete or noisy, categories are coarse, and extra heads push the model towards frequent findings and away from rare but critical ones [7], [8], [17]. In a recent study, Dynamic traceback learning partially advance the semantic consistency by masking or backtracking from generated tokens to visual evidence, illustrating the potential of semantics-aware supervision; still, it relies on proxy curricula that do not directly reflect clinical quality [4].

In this work, we propose a semantic-driven reinforcement learning (SRL) method for MRG that directly optimizes clinical correctness rather than token overlap. We instantiate this framework on a medical large vision-language model (Med-LVLM) to obtain MRG-R1, which is fine-tuned to generate clinically aligned reports with explicit, self-generated reasoning. Instead of supervising individual tokens, we treat the Med-LVLM as a policy that outputs full reports and optimize it with respect to a report-level reward that encodes clinical semantics. This design specifically targets the gaps identified above: it shifts supervision from surface form to clinically meaningful findings, enforces polarity-sensitive agreement with image-grounded evidence, and introduces light structural guidance for interpretable reasoning.

We contribute to SRL by innovating in turning clinical semantics into a stable reinforcement signal and coupling it with Group Relative Policy Optimization (GRPO) [18] to obtain efficient, value-free updates suitable for long-form medical text. For each study, multiple candidate reports are sampled from the current policy; a CheXbert-based reward evaluates their clinical adequacy; and GRPO’s group-wise normalization amplifies the relatively best candidates for that case. In this way, MRG-R1 is explicitly encouraged to produce reports that are both clinically faithful and structurally organized, rather than merely stylistically similar to training texts.

Our main contributions can be summarized as follows:

- Semantic-Driven RL with GRPO for Clinically Aligned MRG. We introduce an SRL framework that casts the Med-LVLM as a report-generation policy and optimizes it using GRPO, moving beyond token-level maximum likelihood. Given a chest X-ray study, the policy samples a small group of candidate reports; GRPO computes group-relative advantages by normalizing rewards within this set, enabling low-variance, value-free policy updates. This directly addresses the mismatch between local token losses and global clinical goals, and provides a stable mechanism to align long-form outputs with clinically

meaningful criteria.

- CheXbert-Guided Clinical Efficacy Reward and Instruction-Driven Explicit Reasoning. To encode clinical semantics, we leverage CheXbert [19] to extract 14-label observations from both generated and reference reports, map them into signed label vectors, and compute a margin-based CheXbert cosine similarity (MCCS) as a report-level reward. MCCS is polarity-sensitive, excludes the noisy “No Finding” dimension, and applies a margin to suppress weak, incidental matches—thereby rewarding accurate coverage and correct polarity while penalizing unsupported or contradictory statements. In parallel, a lightweight format reward—triggered when the model follows a “<think>...</think> → <report>...</report>” structure—encourages explicit, self-generated reasoning without requiring Chain-of-Thought annotations. The total reward is a weighted combination of MCCS and format terms, so clinical correctness remains primary while structural regularity improves interpretability and auditability.
- Comprehensive Empirical Experiments and Ablation Study. Extensive experiments and analyses on the IU X-Ray [20], MIMIC-CXR [21], have validate the clinical efficacy of our method.

II. RELATED WORK

A. Medical Report Generation

Medical report generation aims to produce sectioned narratives that capture anatomy, attributes, and clinically meaningful qualifiers within radiology reports. Beyond fluency, models must ensure factual adequacy, coverage, and consistency at the report level. Historically, this line of work grew out of image captioning [22]: encoder-decoder pipelines learned with maximum-likelihood training mapped visual features to text, with Show and Tell (CNN encoder + RNN decoder) [23] as a canonical example. Early MRG work adapted this recipe to longer, multi-sentence outputs with clinical terminology. Jing et al. [7] introduced hierarchical LSTMs with co-/cross-attention (plus auxiliary disease tags) to better plan sentences and ground wording in chest-X-ray findings. Retrieval-generation hybrids such as HRGR-Agent [10] coupled a generator with a retrieval policy to stabilize long-form outputs, while TieNet [8] jointly learned image-text embeddings for thorax disease classification and produced preliminary reports—tightening visual-textual coupling. With Transformers, MRG shifted beyond recurrent decoders. R2Gen [5] introduced a memory-driven Transformer that caches global cues to manage long-range context across sentences, reporting strong results on IU X-Ray and MIMIC-CXR—but still trained the generator with token-level objectives. Beyond R2Gen, R2GenCMN [24] augments the memory-driven Transformer with cross-modal memory networks to strengthen image-text interactions under teacher forcing, yielding stronger token-level MLE baselines on IU X-Ray/MIMIC-CXR. Subsequent

variants injected prior/posterior knowledge (e.g., PPKED [11]) to mitigate visual/textual biases while keeping the same learning target. Despite architectural differences, these systems largely retained token-level supervision (by using cross-entropy loss), which favors lexico-syntactic similarity over clinically grounded semantics.

Recently, ed-LVLMs have pushed capacity and generality. LLaVA-Med [25] instruction-tunes a vision-language backbone on biomedical image–text pairs for dialogue, captioning, and VQA; Med-Flamingo [26] adapts Open-Flamingo [27] for few-shot generative medical VQA with physician blind review; HuatuoGPT-Vision [28] injects medical visual knowledge at scale into Qwen2-VL [29] and Qwen2.5VL [30] using an LLaVA-style training pipeline; MedGemma-4B/27B [31] adapts Gemma [32] to the medical domain via instruction tuning and evaluated biomedical tasks. CheXagent [33] targets chest-X-ray interpretation and multi-task evaluation via a curated instruction datasets. Radiology-focused variants such as CXR-LLaVA [12] tailor LLaVA [34] to chest X-rays and study zero-/few-shot reporting or recognition; broader “generalist” biomedical models (e.g., BioMedGPT [13]) and radiology foundation efforts (e.g., RadFM [35]) pursue unified pretraining across modalities.

Despite richer prompting, retrieval, and tools, most medical report generators—from memory-driven Transformers (e.g., R2Gen, R2genCMN) to instruction-tuned LVLMs (e.g., LLaVA-Med, HuatuoGPT-Vision)—are still trained with token-level maximum likelihood estimation (MLE), which helps fluency but is only weakly aligned with clinically grounded semantics.

B. Semantic Supervision

To mitigate the mismatch between token-level objectives and clinical goals, a growing amount of work augments report generation with semantic supervision that more directly encodes medical knowledge, grounding, or clinical consistency. Knowledge-centric methods explicitly encode medical structure: KERP [36] learns an abnormality graph then paraphrases into text, improving entity/relationship fidelity, while GSKEET [37] integrates general (graph-based) and specific (retrieved case) knowledge to guide sentence planning. Knowledge graph and knowledge base variants continue this line, for example, Attributed Abnormality Graph (ATAG) [38] and Dynamic Graph Enhanced Contrastive Learning [39] that update graph structure and add contrastive/matching losses for finer semantics.

A complementary thread strengthens image–text grounding via matching or contrastive signals. Co-training a generator with image–text matching (ITM) heads (“self-boosting” [16]) improves clinical alignment by penalizing mismatched pairs. Reinforced Cross-modal Alignment [40] introduces an RL objective over a cross-modal memory to better couple visual and textual cues; and segment-enhanced contrastive learning (MSCL [15]) leverages segmentation (e.g., SAM [41]) to focus alignment on clinically meaningful regions of interest and reduce dataset bias.

Retrieval-assisted systems operationalize this alignment at inference time: X-REM [42] learns a contrastive matching score to retrieve report sentences conditioned on the image, improving grounding and reducing unsupported statements. CXRMate [43] introduces longitudinal semantic rewards that leverage follow-up consistency signals to reduce hallucinations and improve clinically coherent reporting in chest X-rays.

Moving closer to clinically grounded objectives [44], labeler- and information extraction (IE)-based supervision turns clinical extractors into training signals. Clinically Accurate Chest X-ray Report Generation [44] optimizes an RL reward tied to clinical coherence; CheXbert [19] provides a BERT-based automatic labeler widely used to score presence/absence of 14 observations. On the IE side, RadGraph [45] introduces chest-x-ray entity–relation annotations, enabling RadGraph-based rewards that directly optimize factual completeness/correctness. Beyond rewards, Dynamic Traceback Learning [4] regularizes causal consistency by masking/back-tracing across modalities so tokens can be “explained” by visual evidence, reducing spurious correlations.

However, existing semantic supervision is often indirect: contrastive and matching losses provide global alignment, multitask classifiers depend on coarse or noisy labels, and traceback-style methods rely on proxy curricula rather than explicit clinical rewards. This leaves an open need for polarity-sensitive, report-level objectives that can be directly optimized during generation.

C. Reinforcement Learning

Post-training for LLMs/LVLMs increasingly relies on preference-based objectives [46], [47]. The standard Reinforcement Learning from Human Feedback (RLHF) [46] recipe fits a reward model from human comparisons and optimizes the policy with Proximal Policy Optimization (PPO) [48] under a Kullback–Leibler (KL) divergence [49] constraint—popularized by InstructGPT—with PPO’s clipped surrogate providing stable on-policy updates. To cut human labeling, RLAIF/Constitutional AI [47] uses AI feedback and rule-based critiques. Direct Preference Optimization (DPO) [50] simplifies RLHF by dropping the learned reward/value loop and directly fitting to preference pairs. GRPO [18] computes group-relative advantages across multiple sampled responses—value-free and memory-light—and improves reasoning performance. Beyond DPO/GRPO, Odds Ratio Preference Optimization (ORPO) [51] removes the reference model, and Kahneman–Tversky Optimization (KTO) [52] aligns with only binary desirability signals via a prospect-theoretic objective.

Reinforcement learning has long been central to image captioning, where sequence-level objectives are optimized to bridge the gap between likelihood training and non-differentiable evaluation metrics. MIXER [53] anneals from teacher forcing to sampled decoding and applies REINFORCE [54] to optimize sequence metrics (BLEU

[55]/ROUGE [56]), directly addressing exposure bias and loss-metric mismatch. SCST [57] reduces variance by using the model’s test-time greedy caption as the baseline, yielding stable optimization of CIDEr [58]/BLEU [55] without training an extra critic. Subsequent work optimizes SPIDER (SPICE+CIDEr) [59] via policy gradients and develops actor-critic and embedding-reward variants to better couple captions with visual semantics. More recent trends expand or replace the reward: CLIP-based [60] rewards promote recognizability and fine-grained distinctiveness, and PACScore [61] serves as a learned, human-correlated evaluator increasingly used as a training target or diagnostic. In parallel, RL-free sequence objectives have emerged, for example, DiCO [62] distills CLIP/PAC preferences directly into the captioner, and DMO [63] performs offline, reward-weighted augmentation—offering compute-efficient alternatives to on-policy RL while still pursuing metric fidelity.

Prior work thus demonstrates the value of sequence-level and preference-based optimization, but has rarely targeted clinically grounded rewards for long-form radiology reports. We build on GRPO in this setting, coupling it with a rule/labeler-based clinical reward to align Med-LVLMs with report-level medical correctness.

III. METHOD

We cast post-training for MRG as reinforcement learning over a clinically grounded, report-level reward. As shown in Figure 1 given a chest X-ray, the Med-LVLM (policy) samples multiple candidate reports; CheXbert-derived label vectors define a margin-based cosine reward (MCCS), and a lightweight format reward checks the `<think>→<report>` structure. These rewards are combined within groups and optimized via GRPO under a KL constraint to a reference policy. We fine-tune the LVLM with GRPO [18], a value-free, group-wise policy-gradient method selected for its stability and compute efficiency when optimizing sequence-level, report-level clinical rewards. The optimization signal is a CheXbert-guided reward that scores agreement across 14 chest-x-ray observations between the generated report and the reference, providing direct supervision on clinical content and reducing the reliance on n-gram overlap. We next detail (i) the GRPO training loop—sampling, group-relative advantage computation, and update rule. (ii) the reward functions, including the CheXbert margin-cosine design and its aggregation at the report level.

A. Group Relative Policy Optimization (GRPO)

GRPO [18] is a PPO-style [48] post-training algorithm that optimizes reward-defined objectives instead of pure likelihood. In our setting, the LVLM is treated as a policy that generates full reports, and GRPO updates this policy using group-relative advantages computed from our clinical rewards. We leverage this to bias generation toward clinically aligned report-level targets, providing direct supervision on semantic fidelity beyond token overlap.

GRPO is closely related to PPO but differs in two key aspects: first, GRPO estimates the advantage using group-based estimation rather than a value function; second, it uses fixed task-specific reward functions (here, CheXbert-based and format rewards) instead of a learned value network.

Let $P(Q)$ denote the training set of inputs (“studies”); a single input is $q \in P(Q)$. We write $\pi_{\theta_{\text{old}}}$ and $\pi_{\theta_{\text{new}}}$ for the old policy (used to sample responses in the current update) and the current policy (parameters being optimized), respectively. A complete response o means the full generated report for q . We also use a frozen reference policy $\pi_{\theta_{\text{ref}}}$, to regularize updates. Let G be the group size, the number of responses sampled per input q at each iteration, yielding $\{o_i\}_{i=1}^G$.

The GRPO objective is

$$\begin{aligned} J_{\text{GRPO}}(\theta) = & \mathbb{E}_{q \sim P(Q), \{o_i\}_{i=1}^G \sim \pi_{\theta_{\text{old}}}(\cdot|q)} \left[\right. \\ & \left. \frac{1}{G} \sum_{i=1}^G \min \left(\frac{\pi_{\theta_{\text{new}}}(o_i|q)}{\pi_{\theta_{\text{old}}}(o_i|q)} A_i, \right. \right. \\ & \left. \left. \text{clip} \left(\frac{\pi_{\theta_{\text{new}}}(o_i|q)}{\pi_{\theta_{\text{old}}}(o_i|q)}, 1-\epsilon, 1+\epsilon \right) A_i \right) \right. \\ & \left. - \beta D_{\text{KL}}(\pi_{\theta_{\text{new}}} \parallel \pi_{\theta_{\text{ref}}}) \right] \end{aligned} \quad (1)$$

Here, the policy ratio $\frac{\pi_{\theta_{\text{new}}}(o_i|q)}{\pi_{\theta_{\text{old}}}(o_i|q)}$ measures how the new policy probability of o_i changes relative to the old policy; A_i is the estimated advantage for response o_i ; $\epsilon > 0$ is the clipping threshold that limits overly large updates by replacing the raw ratio with its clipped version; and $D_{\text{KL}}(P\|Q)$ is the KL divergence [49] between the new policy and the reference policy, scaled by $\beta \geq 0$ to control policy drift. Intuitively, the “*min*” enforces the clipped surrogate familiar from PPO, while the KL term keeps the updated policy close to $\pi_{\theta_{\text{ref}}}$.

Unlike PPO—which estimates A_i via a learned value function/critic—GRPO computes A_i within the sampled group for the same input to avoid value estimation. Concretely, with rewards $r_i = R(q, o_i)$ from our rule/labeler-based clinical reward R , we use a normalized, within-group advantage

$$\begin{aligned} \bar{r} &= \frac{1}{G} \sum_{i=1}^G r_i, \\ \sigma_r &= \sqrt{\frac{1}{G} \sum_{i=1}^G (r_i - \bar{r})^2 + \epsilon}, \\ A_i &= \frac{r_i - \bar{r}}{\sigma_r}. \end{aligned} \quad (2)$$

where \bar{r} and σ_r are the group mean and standard deviation. Here, $\epsilon > 0$ is a small constant for numerical stability; when the group rewards are identical (variance near zero), set ϵ to a value on the order of 10^{-8} – 10^{-6} . This relative construction compares candidates conditioned on

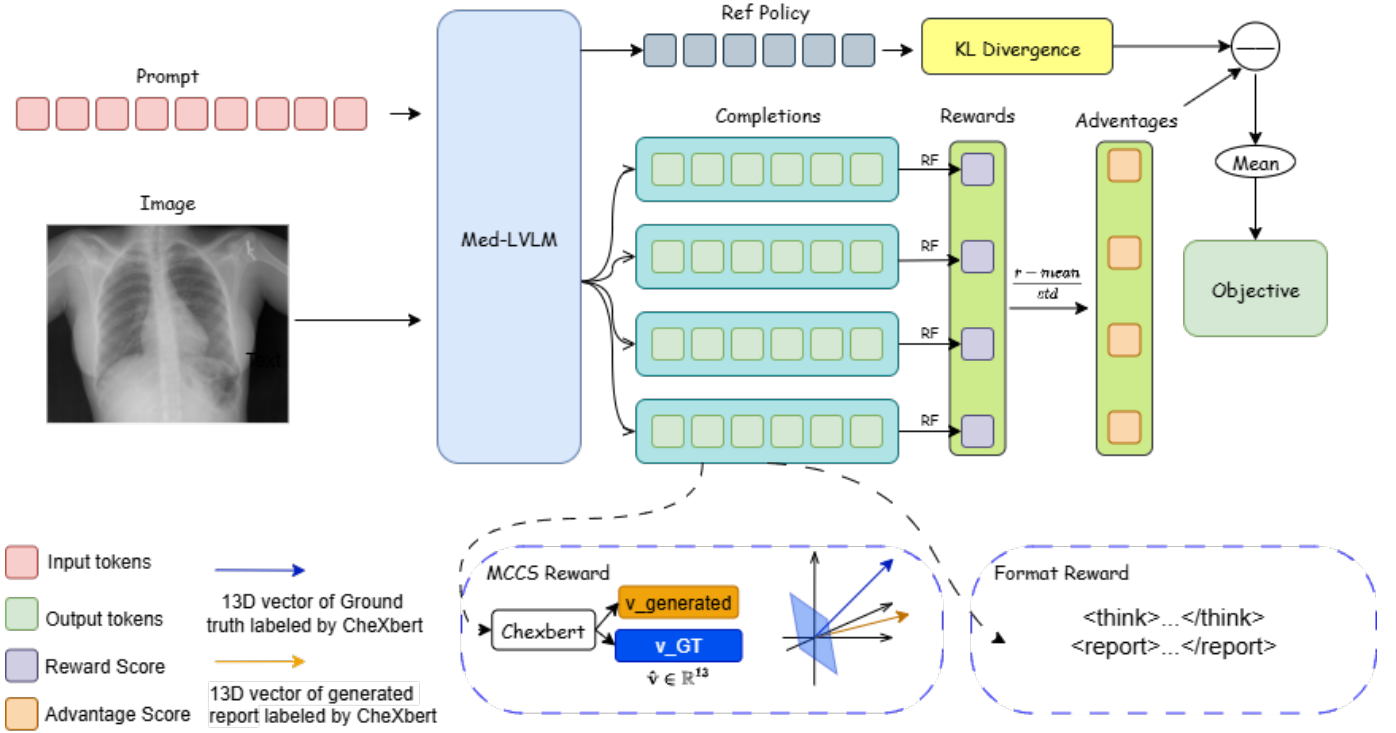


Fig. 1. Overview of SRL. For each study, the policy samples a group of candidate reports; a margin CheXbert cosine reward (MCCS) and a lightweight format reward are combined to compute group-relative advantages for GRPO updates under a KL constraint to a reference policy.

the same study q . sharpening the learning signal for report-level clinical rewards without training a critic.

B. Reward Functions

1) **Format Reward:** We use a format reward to elicit explicit, auditable reasoning without requiring CoT annotations. The prompt asks the model to place intermediate reasoning inside `<think>...</think>` and the final radiology report inside `<report>...</report>`. A rule-based scorer evaluates only structure: tags must be present, correctly ordered, well-formed (balanced), and non-empty. Outputs that fully comply receive a score of 1, with partial credit for minor violations; otherwise the score is 0. This term is added with a small weight relative to the clinical reward so optimization remains driven by medical correctness. Under GRPO’s group-relative updates, candidates that satisfy the structure reliably obtain higher relative advantages within the same case, teaching the policy to produce a stable two-stage “reasoning → report” format. The benefits are threefold: (i) decoupling thinking from the final narrative, (ii) improving readability and downstream parsing, and (iii) enabling auditability to localize hallucinations or inconsistencies.

2) **Margin CheXbert Cosine Similarity Reward (MCCS):** Beyond enforcing output structure via the format reward, our optimization is driven primarily by a clinically grounded signal that evaluates report-level semantics. We instantiate this signal as a Margin CheXbert Cosine Similarity (MCCS) reward, which converts CheXbert’s 14-label [19]

outputs into signed vectors and rewards their margin-calibrated cosine agreement, providing a continuous target for GRPO. Let CheXbert provide, for each study, a 14-way multi-class label over common chest-X-ray observations (e.g., Atelectasis ... No Finding). We map each observation to a scalar by

$$f(\text{pos}) = 1, f(\text{neg}) = -1, f(\text{uncertain}) = 1, f(\text{blank}) = 0. \quad (3)$$

and construct report-level vectors $\mathbf{z}(y), \mathbf{z}(y^*) \in \mathbb{R}^{13}$ over the 13 disease-specific categories only (exclude No Finding) for the generated report y and the reference y^* .

$$z_j(y) = f(\ell_j(y)), z_j(y^*) = f(\ell_j(y^*)), \quad j = 1, \dots, 13. \quad (4)$$

Mapping uncertain to 1 treats hedged mentions as actionable suspicion rather than neutrality, which matches clinical practice: when radiologists hedge, they are flagging a possible abnormality that warrants attention. By contrast, blank is 0, reflecting true omission. This choice biases the reward toward sensitivity—it favors correctly surfacing potential findings and still penalizes polarity reversals (positive vs. negative) most strongly via the signed embedding. It also discourages “safe” under-calling: labeling everything as uncertain no longer evades penalties if the reference is negative (-1) or omitted (0), and it earns credit only when uncertainty aligns with a true or suspected abnormality. We also exclude the No Finding dimension from the cosine similarity. In CheXbert [19], No Finding is typically set to 1 when all other disease labels

are 0. As a result, it can dominate vector norms and inflate apparent agreement via complementarity, and it is highly sensitive to reporting style or templated omissions, thereby introducing noise. Removing this dimension focuses the signal on per-finding clinical agreement and avoids pseudo-alignment driven by a global catch-all label.

We then measure report-level agreement via cosine similarity

$$\text{CCS}(y, y^*) = \frac{\langle z(y), z(y^*) \rangle}{(\|z(y)\|_2 + \varepsilon)(\|z(y^*)\|_2 + \varepsilon)}, \quad \varepsilon = 10^{-8}. \quad (5)$$

This ε guarantees numerical safety even when one vector is (nearly) zero after our preprocessing (e.g., with the No Finding dimension removed), while leaving values effectively unchanged when norms are in a normal range. To calibrate the signal and emphasize clinically meaningful improvements, we convert cosine similarity to a margin-shaped reward:

$$\text{MCCS}(y, y^*, m) = \max \left(\frac{\text{CCS}(y, y^*) - m}{1 - m}, 0 \right), \quad m \in (-1, 1). \quad (6)$$

This piecewise-linear shaping has three advantages. (i) Margin filtering. Scores at or below m yield zero reward, suppressing weak alignments (e.g., incidental overlap) and focusing learning on clinically aligned matches. (ii) Dynamic-range normalization. The division by $(1 - m)$ maps $\text{CCS} \in [m, 1]$ to $[0, 1]$, ensuring comparable reward scales across studies and increasing within-group variance when m is moderate—beneficial for GRPO’s group-relative advantages. (iii) Stable gradients. The linear slope $1/(1 - m)$ avoids early saturation near high similarity and provides smooth, interpretable shaping; $\text{MCCS} = 1$ if and only if the two label vectors coincide up to positive scaling.

In all cases, MCCS acts as a continuous, clinically grounded reward at the report level, providing partial credit for near matches and stronger penalties for polarity mistakes than for uncertainty/omission, thereby aligning optimization with clinical correctness rather than token overlap.

IV. EXPERIMENTAL SETUP

A. Datasets

MIMIC-CXR [21] contains 473,057 chest X-ray images and 227,835 radiology reports. For comparison with prior works, we adopt the split provided by MIMIC-CXR with approximately 222.8k/1.8k/3.3k samples for training/validation/test following [6], [37]. IU X-Ray [20] comprises 7,470 images and 3,955 reports. We follow [5], [6] and use a 70/10/20 train/validation/test split. Unless otherwise noted, multi-view studies (reports associated with multiple images) are treated as multiple image-report pairs, with each image paired to the same report and counted as a separate sample.

B. Implementation Details

All experiments are conducted on 2×NVIDIA A100 GPUs. We fine-tune HuatuoGPT-Vision-7B-Qwen2.5VL¹ [28], a Qwen2.5-VL-based [30] vision-language model further trained on medical image–text and instruction data. We adopt parameter-efficient LoRA tuning [64] (rank 128, $\alpha = 256$, dropout 0.05) on attention and MLP projections, with FlashAttention-2 [65] and bfloat16 for memory efficiency. Optimization uses 8-bit AdamW [66] with learning rate 5×10^{-6} , $(\beta_1, \beta_2) = (0.9, 0.99)$, weight decay 0.1, cosine decay with 10% warm-up, gradient clipping at 0.1, effective batch size 16, and 1 training epoch. We apply DeepSpeed ZeRO-1 [67] for optimizer sharding. For GRPO, each input samples $G = 4$ candidate reports; group-relative advantages are computed within the group, and, when combining rewards, the total reward is a weighted sum of clinical (0.75) and format (0.25) terms.

C. Evaluation Metrics

We evaluated the quality of generated reports using clinical efficacy (CE) metrics that reflect factual correctness rather than stylistic similarity. Specifically, we adopt CheXbert-based precision, recall, and F1 computed over 14 chest X-ray observations defined by CheXbert, following the standard evaluation protocol in prior work [4], [19], [33], [37]. In contrast, conventional NLG metrics such as BLEU, ROUGE, and CIDEr primarily reward n-gram overlap and template reuse, which often obscure factual adequacy and fail to penalize polarity errors. Multiple studies have shown that such lexical metrics correlate weakly with radiologists’ judgments of factual accuracy, whereas CE metrics better track clinically relevant errors [68]–[70].

D. Baselines

In this study, we compare MRG-R1 with three families of baselines in IU X-Ray and MIMIC-CXR, using code / checkpoints released when available and retraining with the authors’ settings otherwise. (A) Token-level MLE generators: R2Gen [5] and R2GenCMN [24], representative encoder - decoder / transformer models trained under teacher forcing. (B) Instruction-tuned medical LLMs: BioMedGPT [13], LLaVA-Med [25], CheXagent [33], HuatuoGPT-Vision [28], and MedGemma-4B/27B [31], evaluated under a uniform prompting and decoding setup without additional fine-tuning on our splits to probe zero / few shot reporting ability and domain alignment. (C) Semantic supervision: DTrace [4], DCL [39], GSKEET [37], CXRMate [43], and RadFM [35], which inject clinical semantics through traceback, contrastive / matching, knowledge graphs or radiology-focused pre-training. Note that some baselines (e.g., CheXagent, MedGemma) are instruction-tuned on substantially broader medical

¹<https://huggingface.co/FreedomIntelligence/HuatuoGPT-Vision-7B-Qwen2.5VL>

corpora beyond MIMIC-CXR and IU X-Ray, and their performance may partly reflect pretraining coverage rather than architecture alone, therefore we treat them as strong external baselines rather than strictly comparable models.

V. RESULTS

A. Quantitative Analysis

In this study, we compared our method against existing report generation models on IU-Xray and MIMIC-CXR.

Across both datasets, our MRG-R1 delivered strong clinical efficacy (CE), achieving state-of-the-art performance on IU X-Ray and competitive results on MIMIC-CXR. On IU X-Ray, MRG-R1 attained the highest $F1=51.88$, edging out classical encoder-decoder baselines such as R2GenCMN (50.53) and matching the top LVLM-style systems (e.g., CheXagent 51.15). The gains were from a balanced improvement in both precision (50.86) and recall (52.98), indicating that SRL with GRPO improved sensitivity to clinically salient findings—key abnormalities and attributes that are critical for radiological assessment and decision-making—while maintaining a low rate of false positives.

On MIMIC-CXR, MRG-R1 achieves $F1=40.39$, which is competitive with recent medical LVLMs (e.g., MedGemma-4B 41.08) and clearly above classic MLE baselines such as R2GenCMN (27.8). Notably, MRG-R1 exhibited higher precision (45.32) than MedGemma-4B (40.77) but lower recall (37.70 vs. 41.40). While CheXagent and MedGemma performed well, we suggest that part of the gains may reflect wider pretraining corpora beyond MIMIC-CXR/IU X-Ray rather than architecture alone. consistent with prior radiology foundation model studies that attribute improvements primarily to large-scale domain-specific pretraining. Compared with instruction-tuned or generalist LVLMs (e.g., LLaVA-Med, BioMedGPT), the CE advantage for our MRG-R1 was substantial, underscoring the benefit of optimizing a clinical reward rather than relying solely on token-level imitation or generic instruction tuning.

We further observed that methods injecting semantic signals without RL (e.g., DTrace’s traceback supervision; CXRMate’s longitudinal semantic reward) yielded stronger CE than early MLE systems, but MRG-R1 remained competitive or superior on average while using a compute-efficient, value-free GRPO objective.

B. Qualitative Analysis

We compared report outputs on representative IU X-Ray and MIMIC-CXR studies (Figures 2 - 3). Both examples illustrate four dimensions that drive clinical utility: (i) polarity handling meaning whether the report states the presence or absence of important abnormalities accurately, (ii) handling of uncertainty where equivocal findings are expressed as suspicion rather than definite statements, (iii) the balance between omissions and hallucinations, avoiding both missing critical findings and introducing

unsupported ones , and (iv) structural coherence where the report is organized in a clear radiology-style format that separates reasoning from conclusions.

On IU X-Ray (Fig.2), the reference emphasizes normal lungs and pleura with a heart size at the upper limit of normal. MRG-R1’s think→report format yields concise itemized statements that preserve correct negatives (no pneumothorax/effusion/consolidation) and a near-normal cardiac size, aligning closely with the ground truth. Several baselines deviate from this: MedGemma-4B hallucinates cardiomegaly which is a polarity error, R2GenCMN also includes extraneous skeletal descriptions that are not central to the target findings, and instruction-tuned LVLMs (e.g., LLaVA-Med) generate fluent but generic prose that fail to specify required clinical elements.

On MIMIC-CXR (Fig.3), the ground truth report documents cardiomegaly, pulmonary edema, and likely effusions as the abnormality. MRG-R1 captures all three abnormalities with consistent polarity, while CheXagent omitted effusion which is polarity inversion, R2GenCMN produced a more vague description of cardiac size that did not clearly reflect cardiomegaly. And BioMedGPT emphasizes line positions while missing pathology (omission). MedGemma-4B identified edema/cardiomegaly but was less reliable on effusion. These patterns are consistent with our quantitative CE results, showing fewer polarity errors and improved alignment with reference findings.

C. Ablation Studies

In this section, we conducted ablation studies on our proposed SRL using the IU X-Ray and MIMIC-CXR dataset to assess the contribution of each component in our method.

We ablate SRL on both datasets to analyze the contribution of each component (Table II). (1) supervised fine-tuning (SFT, cross-entropy), (2) text-level NLG rewards (BLEU/ROUGE/CIDEr), (3) a format-only reward that enforces a $\langle\text{think}\rangle \rightarrow \langle\text{report}\rangle$ structure (Format), (4) a clinical reward via report-level CE-F1 (with/without Format), and (5) our margin CheXbert cosine similarity (MCCS, with/without Format). This sequence disentangles stylistic supervision, structural guidance, and clinically grounded objectives.

Relative to Base, optimizing purely lexical NLG rewards (+NLG) improves fluency but yields limited clinical efficacy (CE): $F1$ rises only to 22.97 on IU X-Ray and 12.72 on MIMIC-CXR, consistent with the weak linkage between n-gram overlap and factual correctness. Replacing the objective with a clinical signal (+CE-F1) substantially improves CE (IU 44.81; MIMIC 29.69), indicating that label-consistency supervision reduces polarity errors and under-calling. A format-only constraint (+Format) increases recall (IU 38.33; MIMIC 25.53) at some cost to precision, while +CE-F1+Format stabilizes negation/uncertainty templates and recovers a strong precision-recall balance (IU $F1=51.35$).

Our MCCS is the most effective shaping in this setting. Compared with CE-F1, MCCS maps CheXbert labels to

Method	IU X-Ray			MIMIC-CXR		
	Precision	Recall	F1	Precision	Recall	F1
R2Gen [5]	50.60*	48.76*	46.99*	33.30	27.30	27.60
R2GenCMN [24]	50.00*	51.07*	50.53*	33.40	27.50	27.80
RadFM [35]	14.27*	11.93*	12.99*	10.03*	12.08*	10.96*
MedGemma-4B [31]	23.93*	22.83*	23.37*	40.77*	41.40*	41.08*
MedGemma-27B [31]	15.40*	21.21*	17.84*	35.18*	36.95*	36.04*
BioMedGPT [13]	36.00*	35.40*	35.50*	29.00*	31.40*	28.60*
LLaVA-Med [25]	18.63*	23.37*	20.73*	26.99*	12.03*	16.64*
CheXagent [33]	50.37*	51.96*	51.15*	45.60*	24.59*	31.95*
HuatuoGPT-Vision [28]	5.87*	7.33*	6.52*	23.67*	16.51*	19.45*
DTrace [4]	—	—	—	41.10	43.60	39.10
DCL [39]	—	—	—	47.10	35.20	37.30
GSKET [37]	—	—	—	45.80	34.80	37.10
CXRMate [43]	28.30	35.10	27.70	43.80	34.90	35.70
MRG-R1 (ours)	50.86	52.98	51.88	45.32	37.70	40.39

TABLE I

CLINICAL EFFICACY (CE) COMPARISON ON IU X-RAY AND MIMIC-CXR. CE IS COMPUTED WITH CHEXBERT OVER THE 14 STANDARD OBSERVATIONS. * DENOTE SCORES IS NOT PROVIDED BY AUTHOR AND REPRODUCED BY OUR. **BOLD** MARKS THE BEST PERFORMANCE PER COLUMN; UNDERLINE MARKS THE SECOND BEST. FOR IU X-RAY, CE IS OBTAINED BY RUNNING CHEXBERT ON BOTH THE GENERATED AND THE GROUND-TRUTH REPORTS, CONSISTENT WITH PRIOR WORK.

Image	Reports	Ground Truth	R2GenCMN	MRG-R1 (ours)
	Ground Truth	1. No pneumothorax, 2. pleural effusion or airspace consolidation. Heart size is upper limits of normal. 3. Pulmonary vasculature appear within normal limits. 4. XXXX XXXX are intact.	1. The heart size and pulmonary vasculature appear within normal limits, the lungs are free of focal airspace disease. 2. No pleural effusion or pneumothorax is seen. 3. degenerative changes are present in the spine.	<report> The lateral chest X-ray (LT LAT) shows clear lung fields, a normal-sized heart, and well-defined mediastinal contours. The bony structures, diaphragm, and pleural spaces are all within normal limits. There are no signs of acute pulmonary pathology, cardiomegaly, or pleural effusion. Pulmonary vasculature appears within normal limits. ... Further clinical correlation is recommended for a complete evaluation. </report>
	BioMedGPT	No acute cardiopulmonary disease. The heart is normal in size and contour. The lungs are clear without evidence of infiltrate. No pneumothorax or effusion	1. The cardiomedastinal silhouette is normal. The lungs are clear. 2. No pleural effusion or pneumothorax is seen.	<report> The chest X-ray is largely unremarkable apart from an enlarged cardiac silhouette, consistent with cardiomegaly. The lung fields are clear without consolidation, effusion, or masses. Bony structures, mediastinum, and diaphragm appear within normal limits. The cardiomegaly may relate to hypertension, valvular disease, cardiomyopathy, or pericardial effusion, and further assessment (e.g., echocardiography) is recommended.

Fig. 2. An example case from IU X-ray (X-ray image) used for inference in MRG qualitative comparisons. The information in the ground truth report is labeled from 1 to 6 and highlighted separately. The generated reports are labeled according to the ground truth report and highlighted with different colors to represent the differences between the generated sequences and the ground truth report: (1)Green-consistent; (2)Red- incorrect information; (3)Unhighlighted-not included in the ground truth.

Image	Reports	Ground Truth	R2GenCMN	MRG-R1 (ours)
	Ground Truth	Portable AP upright chest radiograph obtained. The heart is moderately enlarged and there is diffuse pulmonary edema. Effusions are likely also present.	1. ap portable upright view of the chest overlying ekg leads are present. lung volumes are low limiting assessment. 2. there is diffuse pulmonary edema with probable small bilateral pleura effusions. heart size cannot be assessed. mediastinal contour is grossly unremarkable. bony structures are intact.	<report> 3. The chest X-ray reveals bilateral pleural effusion, moderate cardiomegaly, and patchy lung opacities. These findings suggest fluid accumulation in the pleural space, enlargement of the heart, and possible pulmonary pathology. Further investigation is recommended to determine the underlying causes and appropriate management </report>
	BioMedGPT	Right internal jugular central venous catheter tip terminate in the right atrium unchanged in position compared to prior study	1. Moderate pulmonary edema is present. 2. There is no pneumothorax or pleural effusion. 3. The cardiac and mediastinal silhouettes are stable.	<report> The chest X-ray shows significant bilateral pulmonary edema with an enlarged cardiac silhouette. There is diffuse increased density in both lungs, most marked in the peripheral regions, consistent with cardiogenic pulmonary edema. 1. The heart appears enlarged, suggesting cardiomegaly. The bony structures and mediastinum appear within normal limits. Clinical correlation with history, examination, and further tests (e.g., ECG, blood tests) is required, and additional imaging such as chest CT may be considered if indicated.

Fig. 3. An example case from MIMIC-CXR (X-ray image) used for inference in MRG qualitative comparisons. The information in the ground truth report is labeled from 1 to 3 and highlighted separately. The generated reports are labeled according to the ground truth report and highlighted with different colors to represent the differences between the generated sequences and the ground truth report: (1)Green-consistent; (2)Red- incorrect information; (3)Unhighlighted-not included in the ground truth.

Method	IU X-Ray			MIMIC-CXR		
	Precision	Recall	F1	Precision	Recall	F1
Base	5.87	7.33	6.52	23.67	16.51	19.45
Base + SFT	3.86	7.09	4.99	24.27	15.00	14.64
Base + NLG	41.19	15.93	22.97	24.74	8.56	12.72
Base + CE F1	45.89	43.78	44.81	36.38	25.08	29.69
Base + reasoning	24.21	38.33	29.67	27.71	25.53	26.58
Base + CE F1 + reasoning	50.04	<u>52.73</u>	<u>51.35</u>	33.00	28.87	29.50
Base + MCCS	53.27	46.51	49.66	<u>36.07</u>	44.69	<u>38.67</u>
Base + MCCS + reasoning	<u>50.86</u>	52.98	51.88	45.32	<u>37.70</u>	40.39

TABLE II

ABLATION ON IU X-RAY AND MIMIC-CXR STARTING FROM A ZERO-SHOT HUATUOGPT-VISION-7B (BASE). WE INCREMENTALLY ADD: SUPERVISED FINE-TUNING (SFT, CROSS-ENTROPY), TEXT-LEVEL NLG REWARDS (BLEU+ROUGE+CIDEr), A FORMAT-ONLY REWARD ENFORCING A $\langle\text{THINK}\rangle \rightarrow \langle\text{REPORT}\rangle$ STRUCTURE (FORMAT), A CLINICAL REWARD VIA REPORT-LEVEL CE-F1 (WITH/WITHOUT FORMAT), AND OUR MARGIN CHEXBERT COSINE SIMILARITY (MCCS, WITH/WITHOUT FORMAT). **BOLD** MARKS THE BEST PER COLUMN; UNDERLINE THE SECOND BEST.

signed vectors ($\text{pos} = 1$, $\text{neg} = -1$, $\text{blank} = 0$, $\text{uncertain} = 1$), excludes the catch-all No Finding, and applies a margin that suppresses weak matches. This polarity-sensitive, sequence-level signal widens case-level score separation, which GRPO’s group-relative updates leverage to amplify the best candidate per study. Empirically, +MCCS boosts recall on MIMIC-CXR (44.69; second-best F1 38.67), and +MCCS+Format delivers the best overall CE on both datasets (IU F1 51.88; MIMIC F1 40.39) with the highest MIMIC precision (45.32). These trends support MCCS as a stronger clinical reward than CE-F1 under GRPO and motivate pairing it with a light format constraint for stable long-form generation.

VI. DISCUSSION

Our experiments show that MRG-R1 establishes state-of-the-art clinical alignment on IU-Xray and MIMIC-CXR, confirming the efficacy of reinforcement learning for bridging the gap between vision-language modeling and radiological reasoning. By optimizing report-level, clinically grounded objectives rather than token-wise likelihoods, reinforcement learning enables holistic credit assignment across an entire report. This shift allows the model to align its behaviour with how radiologists actually judge reports—at the level of study-wide consistency and coverage—so that correct affirmations and negations of key findings are rewarded, omissions and unsupported statements are penalized, and precision–recall trade-offs can be shaped directly at the sequence level. In contrast, conventional maximum-likelihood training only reinforces locally probable word sequences, which improves fluency but cannot explicitly encode polarity, coverage, or clinical adequacy of the report as a whole.

The relatively larger improvement observed on IU X-Ray also suggests that GRPO-based post-training can be effective even when supervision is limited. Compared with MIMIC-CXR, IU X-Ray is much smaller and has been reported to exhibit less complicated visual-textual mappings, making it an easier benchmark for report generation. In this setting, optimizing a report-level clinical reward effectively reweights training toward cases and candidate reports that better capture key findings, while down-weighting responses that are clinically uninformative. This leads to richer, clinically meaningful feedback for each labeled study, so that individual training examples contribute more directly to aligning the policy with radiological judgments. As a result, policy updates are more strongly driven by diagnostically meaningful patterns rather than by surface-level token statistics, which helps the model produce clinically consistent reports on IU X-Ray despite its limited size. On the larger and more heterogeneous MIMIC-CXR benchmark, the absolute gains are smaller but still substantial, indicating that the same reinforcement learning scheme remains beneficial even under a more complex data distribution.

We further analyze the contribution of each component through the ablation study in Table II. Starting from the zero-shot HuatuoGPT-Vision base model, conventional supervised fine-tuning with cross-entropy (+SFT) does not improve and can even reduce CE, illustrating that on these datasets MLE primarily reinforces stylistic patterns rather than clinically grounded semantics. When we switch to GRPO but use only NLG metrics as the reward (+NLG), the model learns to adjust style and surface overlap, but CE remains low especially on MIMIC-CXR which confirming that BLEU/ROUGE/CIDEr are not suitable targets for factual correctness in MRG.

The format-only reward (+reasoning), which enforces the "`<think>...</think> → <report>...</report>`" structure without any clinical reward, mainly increases recall by encouraging more explicit mention of potential findings, but this comes at the cost of precision because the model is not penalized for unsupported statements. Introducing a CheXbert-based CE F1 reward (+CE F1) markedly boosts CE over all these variants, and combining it with the format reward (+CE F1 + reasoning) stabilises the negation and uncertainty templates and approaches the performance of the entire model, confirming that label-level supervision is effective in reducing polarity errors and under-calling. However, CE-F1 remains a discrete, aggregate score and provides a relatively coarse learning signal. Replacing it with our MCCS reward (+MCCS) leads to further improvements: by mapping CheXbert labels to signed vectors, excluding the noisy "No Finding" dimension, and applying a margin to suppress weak matches, MCCS offers a smoother, polarity-sensitive, report-level objective that better distinguishes partially correct from clinically problematic outputs. GRPO's group-relative updates can then exploit the larger reward spread within each case to amplify the best candidate report. When MCCS is combined with the format reward (+MCCS + reasoning), the model reaches the strongest and most balanced CE across both datasets, aligning clinical content while maintaining a stable, auditable report structure. Taken together, these ablations show that each component plays a distinct role: GRPO enabling sequence-level optimization, clinical rewards steering semantics, and the format reward regularizing structure and that the proposed MCCS-based design provides a more informative and clinically meaningful supervision signal than directly optimizing CE-F1 or purely lexical objectives.

Qualitative comparisons further illuminate how SRL reshapes model behaviour beyond what CE scores alone capture. Across the IU X-Ray and MIMIC-CXR case studies, MRG-R1's reports exhibit more reliable control of polarity—abnormalities that are truly present or absent are described consistently across sentences—indicating that the reward is successfully penalizing internal contradictions rather than simply rewarding fluency. The model also tends to surface clinically important findings instead of defaulting to generic "no acute abnormality" templates, suggesting that sequence-level optimization encourages it to prioritise label-supported observations over safe but uninformative normal statements. Its handling of uncertainty is more calibrated: equivocal patterns are framed as suspicion rather than as definite disease or definite normality, which aligns with the way radiologists hedge when evidence is borderline and reflects the polarity- and uncertainty-aware design of MCCS. The `<think>→<report>` structure additionally makes the reasoning process more transparent; intermediate "thinking" often mirrors the CheXbert label space, while the final report rephrases those decisions into radiology-style prose, providing a natural point for auditing where hallucinations or misinterpretations arise. At the same

time, the residual errors we observe: missed subtle or highly localized findings, incomplete description of devices and lines, and overly conservative summaries in ambiguous cases are concentrated precisely in areas where the current reward is blind or weak, namely phenomena not covered by the 14-label scheme or poorly captured by single-time-point views. This pattern supports the view that MRG-R1 is genuinely aligning to the supervision it receives, rather than memorizing templates: where the reward is expressive, behaviour improves in clinically meaningful ways; where the reward is coarse, limitations remain.

This work has several limitations that point to directions for future research. First, the reward relies on CheXbert over 14 chest X-ray observations, which provides a clinically relevant but coarse signal that is insensitive to device placement, fine-grained anatomical localization, and temporal change. Second, our experiments focus on single-modality chest X-ray data, and the GRPO updates operate on groups of sampled reports, which cannot correct subtle findings that are consistently missed across all candidates. Third, our evaluation is based on automatic metrics without large-scale blinded assessment by radiologists, so further validation is needed before deployment in safety-critical workflows. Future work should therefore explore richer and more granular supervision signals (including calibrated handling of uncertainty and severity), extend the framework to multi-organ, multi-modality and longitudinal settings, and investigate hybrid reward designs that combine automatic labelers with targeted expert feedback. In practice, we envision MRG-R1-style models being integrated as decision-support tools for report drafting and quality assurance—flagging potential polarity errors, omissions, or inconsistencies—rather than replacing radiologist judgment, providing a foundation for progressively more reliable and clinically aligned medical report generation systems.

VII. CONCLUSION

In this paper, we addressed the gap between token-level objectives and clinical goals in medical report generation by introducing a semantic-driven reinforcement learning (SRL) method that fine-tunes LVLMs with Group Relative Policy Optimization (GRPO) and a Margin CheXbert Cosine Similarity (MCCS) reward, complemented by a lightweight format reward. On MIMIC-CXR and IU X-Ray, the resulting MRG-R1 system achieves consistent gains on CheXbert-based precision, recall, and F1, with fewer polarity mistakes and fewer unsupported statements; training remains stable and compute-efficient due to GRPO's group-relative advantages and value-free updates. Ablations validate the contribution of medical-domain initialization, MCCS shaping, and the format constraint. Future work will focus on the reward with structured clinical signals, expand to multi-organ and multi-image-modalities settings, thereby further advancing our capabilities in intelligent healthcare systems.

REFERENCES

[1] T. C. Kwee and R. M. Kwee, "Workload of diagnostic radiologists in the foreseeable future based on recent scientific advances: growth expectations and role of artificial intelligence," *Insights into imaging*, vol. 12, no. 1, p. 88, 2021.

[2] Ö. Kasalak, H. Alnahwi, R. Toxopeus, J. P. Pennings, D. Yakar, and T. C. Kwee, "Work overload and diagnostic errors in radiology," *European Journal of Radiology*, vol. 167, p. 111032, 2023.

[3] Y. Peng, X. Wang, L. Lu, M. Bagheri, R. Summers, and Z. Lu, "Negbio: a high-performance tool for negation and uncertainty detection in radiology reports," *AMIA Summits on Translational Science Proceedings*, vol. 2018, p. 188, 2018.

[4] S. Ye, M. Meng, M. Li, D. Feng, U. Naseem, and J. Kim, "Dynamic traceback learning for medical report generation," *arXiv preprint arXiv:2401.13267*, 2024.

[5] Z. Chen, Y. Song, T.-H. Chang, and X. Wan, "Generating radiology reports via memory-driven transformer," *arXiv preprint arXiv:2010.16056*, 2020.

[6] Z. Chen, Y. Shen, Y. Song, and X. Wan, "Cross-modal memory networks for radiology report generation," *arXiv preprint arXiv:2204.13258*, 2022.

[7] B. Jing, P. Xie, and E. Xing, "On the automatic generation of medical imaging reports," *arXiv preprint arXiv:1711.08195*, 2017.

[8] X. Wang, Y. Peng, L. Lu, Z. Lu, and R. M. Summers, "Tienet: Text-image embedding network for common thorax disease classification and reporting in chest x-rays," in *Proceedings of the IEEE conference on computer vision and pattern recognition*, 2018, pp. 9049–9058.

[9] Y. Miura et al., "Improving factual completeness and consistency of image-to-text radiology report generation," in *Findings of the Association for Computational Linguistics: EMNLP 2021*, 2021.

[10] Y. Li, X. Liang, Z. Hu, and E. P. Xing, "Hybrid retrieval-generation reinforced agent for medical image report generation," *Advances in neural information processing systems*, vol. 31, 2018.

[11] F. Liu, X. Wu, S. Ge, W. Fan, and Y. Zou, "Exploring and distilling posterior and prior knowledge for radiology report generation," in *Proceedings of the IEEE/CVF conference on computer vision and pattern recognition*, 2021, pp. 13753–13762.

[12] S. Lee, J. Youn, H. Kim, M. Kim, and S. H. Yoon, "Cxr-llava: a multimodal large language model for interpreting chest x-ray images," *European Radiology*, pp. 1–13, 2025.

[13] K. Zhang, R. Zhou, E. Adhikarla, Z. Yan, Y. Liu, J. Yu, Z. Liu, X. Chen, B. D. Davison, H. Ren et al., "A generalist vision-language foundation model for diverse biomedical tasks," *Nature Medicine*, pp. 1–13, 2024.

[14] M. Li, H. Lin, L. Qiu, X. Liang, L. Chen, A. Elsaddik, and X. Chang, "Contrastive learning with counterfactual explanations for radiology report generation," in *European Conference on Computer Vision*. Springer, 2024, pp. 162–180.

[15] R. Zhao, X. Wang, H. Dai, P. Gao, and P. Li, "Medical report generation based on segment-enhanced contrastive representation learning," in *CCF International Conference on Natural Language Processing and Chinese Computing*. Springer, 2023, pp. 838–849.

[16] Z. Wang, L. Zhou, L. Wang, and X. Li, "A self-boosting framework for automated radiographic report generation," in *Proceedings of the IEEE/CVF Conference on Computer Vision and Pattern Recognition*, 2021, pp. 2433–2442.

[17] Z. Wang, H. Han, L. Wang, X. Li, and L. Zhou, "Automated radiographic report generation purely on transformer: A multi-criteria supervised approach," *IEEE Transactions on Medical Imaging*, vol. 41, no. 10, pp. 2803–2813, 2022.

[18] Z. Shao, P. Wang, Q. Zhu, R. Xu, J. Song, X. Bi, H. Zhang, M. Zhang, Y. Li, Y. Wu et al., "Deepseekmath: Pushing the limits of mathematical reasoning in open language models," *arXiv preprint arXiv:2402.03300*, 2024.

[19] A. Smit, S. Jain, P. Rajpurkar, A. Pareek, A. Y. Ng, and M. P. Lungren, "Chexbert: combining automatic labelers and expert annotations for accurate radiology report labeling using bert," *arXiv preprint arXiv:2004.09167*, 2020.

[20] D. Demner-Fushman, M. D. Kohli, M. B. Rosenman, S. E. Shooshan, L. Rodriguez, S. Antani, G. R. Thoma, and C. J. McDonald, "Preparing a collection of radiology examinations for distribution and retrieval," *Journal of the American Medical Informatics Association*, vol. 23, no. 2, pp. 304–310, 2015.

[21] A. E. Johnson, T. J. Pollard, S. J. Berkowitz, N. R. Greenbaum, M. P. Lungren, C.-y. Deng, R. G. Mark, and S. Horng, "Mimic-cxr, a de-identified publicly available database of chest radiographs with free-text reports," *Scientific data*, vol. 6, no. 1, p. 317, 2019.

[22] V. Ordonez, G. Kulkarni, and T. L. Berg, "Im2text: Describing images using 1 million captioned photographs," in *Neural Information Processing Systems (NIPS)*, 2011.

[23] O. Vinyals, A. Toshev, S. Bengio, and D. Erhan, "Show and tell: A neural image caption generator," in *Proceedings of the IEEE conference on computer vision and pattern recognition*, 2015, pp. 3156–3164.

[24] Z. Chen, Y. Shen, Y. Song, and X. Wan, "Generating radiology reports via memory-driven transformer," in *Proceedings of the Joint Conference of the 59th Annual Meeting of the Association for Computational Linguistics and the 11th International Joint Conference on Natural Language Processing*, Aug. 2021.

[25] C. Li, C. Wong, S. Zhang, N. Usuyama, H. Liu, J. Yang, T. Naumann, H. Poon, and J. Gao, "Llava-med: Training a large language-and-vision assistant for biomedicine in one day," *Advances in Neural Information Processing Systems*, vol. 36, pp. 28541–28564, 2023.

[26] M. Moor, Q. Huang, S. Wu, M. Yasunaga, Y. Dalmia, J. Leskovec, C. Zakka, E. P. Reis, and P. Rajpurkar, "Medflamingo: a multimodal medical few-shot learner," in *Machine Learning for Health (ML4H)*. PMLR, 2023, pp. 353–367.

[27] A. Awadalla, I. Gao, J. Gardner, J. Hessel, Y. Hanafy, W. Zhu, K. Marathe, Y. Bitton, S. Gadre, S. Sagawa et al., "Openflamingo: An open-source framework for training large autoregressive vision-language models," *arXiv preprint arXiv:2308.01390*, 2023.

[28] J. Chen, C. Gui, R. Ouyang, A. Gao, S. Chen, G. H. Chen, X. Wang, R. Zhang, Z. Cai, K. Ji et al., "Huatuogpt-vision, towards injecting medical visual knowledge into multimodal llms at scale," *arXiv preprint arXiv:2406.19280*, 2024.

[29] P. Wang, S. Bai, S. Tan, S. Wang, Z. Fan, J. Bai, K. Chen, X. Liu, J. Wang, W. Ge et al., "Qwen2-vl: Enhancing vision-language model's perception of the world at any resolution," *arXiv preprint arXiv:2409.12191*, 2024.

[30] S. Bai, K. Chen, X. Liu, J. Wang, W. Ge, S. Song, K. Dang, P. Wang, S. Wang, J. Tang et al., "Qwen2. 5-vl technical report," *arXiv preprint arXiv:2502.13923*, 2025.

[31] A. Sellergren, S. Kazemzadeh, T. Jaroensri, A. Kiraly, M. Traverse, T. Kohlberger, S. Xu, F. Jamil, C. Hughes, C. Lau et al., "Medgemma technical report," *arXiv preprint arXiv:2507.05201*, 2025.

[32] G. Team, A. Kamath, J. Ferret, S. Pathak, N. Vieillard, R. Merhej, S. Perrin, T. Matejovicova, A. Ramé, M. Rivière et al., "Gemma 3 technical report," *arXiv preprint arXiv:2503.19786*, 2025.

[33] Z. Chen, M. Varma, J.-B. Delbrouck, M. Paschali, L. Blanke-meier, D. Van Veen, J. M. J. Valanarasu, A. Youssef, J. P. Cohen, E. P. Reis et al., "Chexagent: Towards a foundation model for chest x-ray interpretation," *arXiv preprint arXiv:2401.12208*, 2024.

[34] H. Liu, C. Li, Q. Wu, and Y. J. Lee, "Visual instruction tuning," *Advances in neural information processing systems*, vol. 36, pp. 34892–34916, 2023.

[35] C. Wu, X. Zhang, Y. Zhang, H. Hui, Y. Wang, and W. Xie, "Towards generalist foundation model for radiology by leveraging web-scale 2d&3d medical data," *Nature Communications*, vol. 16, no. 1, p. 7866, 2025.

[36] C. Y. Li, X. Liang, Z. Hu, and E. P. Xing, "Knowledge-driven encode, retrieve, paraphrase for medical image report generation," in *Proceedings of the AAAI conference on artificial intelligence*, vol. 33, no. 01, 2019, pp. 6666–6673.

[37] S. Yang, X. Wu, S. Ge, S. K. Zhou, and L. Xiao, "Knowledge matters: Chest radiology report generation with general and

specific knowledge," *Medical image analysis*, vol. 80, p. 102510, 2022.

[38] S. Yan, W. K. Cheung, K. Chiu, T. M. Tong, K. C. Cheung, and S. See, "Attributed abnormality graph embedding for clinically accurate x-ray report generation," *IEEE Transactions on Medical Imaging*, vol. 42, no. 8, pp. 2211–2222, 2023.

[39] M. Li, B. Lin, Z. Chen, H. Lin, X. Liang, and X. Chang, "Dynamic graph enhanced contrastive learning for chest x-ray report generation," in *Proceedings of the IEEE/CVF Conference on Computer Vision and Pattern Recognition*, 2023, pp. 3334–3343.

[40] H. Qin and Y. Song, "Reinforced cross-modal alignment for radiology report generation," in *Findings of the Association for Computational Linguistics: ACL 2022*, 2022, pp. 448–458.

[41] A. Kirillov, E. Mintun, N. Ravi, H. Mao, C. Rolland, L. Gustafson, T. Xiao, S. Whitehead, A. C. Berg, W.-Y. Lo et al., "Segment anything," in *Proceedings of the IEEE/CVF international conference on computer vision*, 2023, pp. 4015–4026.

[42] J. Jeong, K. Tian, A. Li, S. Hartung, S. Adithan, F. Behzadi, J. Calle, D. Osayande, M. Pohlen, and P. Rajpurkar, "Multimodal image-text matching improves retrieval-based chest x-ray report generation," in *Medical Imaging with Deep Learning. PMLR*, 2024, pp. 978–990.

[43] A. Nicolson, J. Dowling, D. Anderson, and B. Koopman, "Longitudinal data and a semantic similarity reward for chest x-ray report generation," *Informatics in Medicine Unlocked*, vol. 50, p. 101585, 2024.

[44] G. Liu, T. Hsu, M. McDermott, W. Boag, W. Weng, P. Szolovits, and M. Ghassemi, "Clinically accurate chest x-ray report generation. corr," *arXiv preprint arXiv:1904.02633*, 2019.

[45] S. Jain, A. Agrawal, A. Saporta, S. Q. Truong, D. N. Duong, T. Bui, P. Chambon, Y. Zhang, M. P. Lungren, A. Y. Ng et al., "Radgraph: Extracting clinical entities and relations from radiology reports," *arXiv preprint arXiv:2106.14463*, 2021.

[46] L. Ouyang, J. Wu, X. Jiang, D. Almeida, C. Wainwright, P. Mishkin, C. Zhang, S. Agarwal, K. Slama, A. Ray et al., "Training language models to follow instructions with human feedback," *Advances in neural information processing systems*, vol. 35, pp. 27730–27744, 2022.

[47] Y. Bai, S. Kadavath, S. Kundu, A. Askell, J. Kernion, A. Jones, A. Chen, A. Goldie, A. Mirhoseini, C. McKinnon et al., "Constitutional ai: Harmlessness from ai feedback," *arXiv preprint arXiv:2212.08073*, 2022.

[48] J. Schulman, F. Wolski, P. Dhariwal, A. Radford, and O. Klimov, "Proximal policy optimization algorithms," *arXiv preprint arXiv:1707.06347*, 2017.

[49] S. Kullback, "Kullback-leibler divergence," *Tech. Rep.*, 1951.

[50] R. Rafailov, A. Sharma, E. Mitchell, C. D. Manning, S. Ermon, and C. Finn, "Direct preference optimization: Your language model is secretly a reward model," *Advances in neural information processing systems*, vol. 36, pp. 53728–53741, 2023.

[51] J. Hong, N. Lee, and J. Thorne, "Orpo: Monolithic preference optimization without reference model," *arXiv preprint arXiv:2403.07691*, 2024.

[52] K. Ethayarajh, W. Xu, N. Muennighoff, D. Jurafsky, and D. Kiela, "Kto: Model alignment as prospect theoretic optimization," *arXiv preprint arXiv:2402.01306*, 2024.

[53] M. Ranzato, S. Chopra, M. Auli, and W. Zaremba, "Sequence level training with recurrent neural networks," *arXiv preprint arXiv:1511.06732*, 2015.

[54] R. J. Williams, "Simple statistical gradient-following algorithms for connectionist reinforcement learning," *Machine learning*, vol. 8, no. 3, pp. 229–256, 1992.

[55] K. Papineni, S. Roukos, T. Ward, and W.-J. Zhu, "Bleu: a method for automatic evaluation of machine translation," in *Proceedings of the 40th annual meeting of the Association for Computational Linguistics*, 2002, pp. 311–318.

[56] C.-Y. Lin, "Rouge: A package for automatic evaluation of summaries," in *Text summarization branches out*, 2004, pp. 74–81.

[57] S. J. Rennie, E. Marcheret, Y. Mroueh, J. Ross, and V. Goel, "Self-critical sequence training for image captioning," in *Proceedings of the IEEE conference on computer vision and pattern recognition*, 2017, pp. 7008–7024.

[58] R. Vedantam, C. Lawrence Zitnick, and D. Parikh, "Cider: Consensus-based image description evaluation," in *Proceedings of the IEEE conference on computer vision and pattern recognition*, 2015, pp. 4566–4575.

[59] S. Liu, Z. Zhu, N. Ye, S. Guadarrama, and K. Murphy, "Improved image captioning via policy gradient optimization of spider," in *Proceedings of the IEEE international conference on computer vision*, 2017, pp. 873–881.

[60] J. Cho, S. Yoon, A. Kale, F. Dernoncourt, T. Bui, and M. Bansal, "Fine-grained image captioning with clip reward," *arXiv preprint arXiv:2205.13115*, 2022.

[61] S. Sarto, M. Barraco, M. Cornia, L. Baraldi, and R. Cucchiara, "Positive-Augmented Contrastive Learning for Image and Video Captioning Evaluation," in *Proceedings of the IEEE/CVF Conference on Computer Vision and Pattern Recognition*, 2023.

[62] N. Moratelli, D. Caffagni, M. Cornia, L. Baraldi, and R. Cucchiara, "Revisiting image captioning training paradigm via direct clip-based optimization," *arXiv preprint arXiv:2408.14547*, 2024.

[63] T. Takada, Y. Suzuki, H. Takushima, H. Tanoue, H. Sato, A. Kumar, H. Nishihara, T. Hori, and K. Ueki, "Direct metric optimization for image captioning through reward-weighted augmented data utilization," in *Proceedings of the 62nd Annual Meeting of the Association for Computational Linguistics (Volume 1: Long Papers)*, 2024, pp. 8333–8346.

[64] E. J. Hu, Y. Shen, P. Wallis, Z. Allen-Zhu, Y. Li, S. Wang, L. Wang, W. Chen et al., "Lora: Low-rank adaptation of large language models," *ICLR*, vol. 1, no. 2, p. 3, 2022.

[65] T. Dao, D. Fu, S. Ermon, A. Rudra, and C. Ré, "Flashattention: Fast and memory-efficient exact attention with io-awareness," *Advances in neural information processing systems*, vol. 35, pp. 16344–16359, 2022.

[66] I. Loshchilov and F. Hutter, "Decoupled weight decay regularization," *arXiv preprint arXiv:1711.05101*, 2017.

[67] J. Rasley, S. Rajbhandari, O. Ruwase, and Y. He, "Deepspeed: System optimizations enable training deep learning models with over 100 billion parameters," in *Proceedings of the 26th ACM SIGKDD international conference on knowledge discovery & data mining*, 2020, pp. 3505–3506.

[68] F. Yu, M. Endo, R. Krishnan, I. Pan, A. Tsai, E. P. Reis, E. K. U. N. Fonseca, H. M. H. Lee, Z. S. H. Abad, A. Y. Ng et al., "Evaluating progress in automatic chest x-ray radiology report generation. patterns 4, 9 (2023)," 2023.

[69] S. Ostmeier, J. Xu, Z. Chen, M. Varma, L. Blankemeier, C. Bluethgen, A. E. Michalson, M. Moseley, C. Langlotz, A. S. Chaudhari et al., "Green: Generative radiology report evaluation and error notation," *arXiv preprint arXiv:2405.03595*, 2024.

[70] Y. Liu, Z. Wang, Y. Li, X. Liang, L. Liu, L. Wang, and L. Zhou, "Mrscore: Evaluating radiology report generation with llm-based reward system," *arXiv preprint arXiv:2404.17778*, 2024.